Stereoscopic PIV Measurements of the Human Thermal Plume

Abhilash Sankaran*, Thomas Fuchs, Rainer Hain, Christian J. Kähler

Universität der Bundeswehr München
Institute of Fluid Mechanics and Aerodynamics
85577 Neubiberg, Germany
*Corresponding author: abhilash.sankaran@unibw.de

Keywords: Stereoscopic PIV, Human thermal plume, Indoor flow

ABSTRACT

A human thermal plume can contribute significantly towards indoor fluid flo ws. Such flows impact the ventilation system designs like mixing and displacement ventilation. Further, the human thermal plume influences the dispersion of air constituents to and away from the breathing zone. This is also relevant in the transport of respiratory droplets which results in spread of respiratory diseases including COVID-19. One of the general scenarios in many ventilated spaces is the sitting condition which is the focus here. Experiments were performed with a thermal manikin and comparisons were made with a real human. The thermal plume is visualised by Stereoscopic PIV with the visualisation plane located 0.3 m above the head parallel to ground. The results show that the thermal plume from a manikin without breathing function has many similarities in the average flow field above the head compared to a real person. Additionally, the plume axis wandering in time has been observed which resulted in non-axisymmetric flow above the head in both the cases. Various scenarios in case of the real person with and without mask on and talking are presented. In addition, the integral fluxes like volumetric flux and momentum flux are calculated.

1. Introduction

Human thermal plumes can induce a considerable flow in indoor conditions. This leads to the importance of human thermal plumes to the fluid flow behavior in rooms, see Licina et al. (2014). Such flows are important in designing different indoor ventilation systems based on mixing and displacement ventilation. In case of displacement ventilation, it is important to know the volumetric flow contribution from humans as that adds to the driving of the flow to the ventilation system. In case of mixing ventilation, human thermal plumes add primarily to the mixing of the clean and polluted air. For both the systems it is important to have both qualitative and quantitative understanding of the contribution from the thermal plume of a human body. The human thermal plume influences the dispersion of air constituents to and from the breathing zone, see Sun et al. (2021). Hence, this is also relevant in the transport of respiratory aerosol particles which results in spread of respiratory diseases including COVID-19. A sitting position is one of the most

often scenario in many ventilated spaces including offices, classrooms or theaters, to name a few. Therefore, this study focuses on the thermal plume in sitting position. The flow due to breathing and the natural convection due to the body temperature are important factors which modify any internal flows. Typically internal flows are studied and designed either for displacement, mixing or natural ventilation. However, presence of humans changes the flow within the system. The flow can be modified by movement of the humans present or their natural perspiration and thermal boundary layer. In this work, the flow around a thermal manikin isolated from the breathing effect is investigated. Few studies have been conducted on thermal manikin flows and effect of different parameters like clothing, breathing, and body posture, see Koelblen & Bogdan (2015), Zukowska et al. (2012), Zukowska et al. (2011). Thermal plumes above male human subjects were also carried out, see Bogdan et al. (2022). Most of them relied on multiple anemometers measuring the velocity field with a least velocity measurement of $0.05\,\mathrm{m/s}$. PIV measurements have been conducted for indoor flows Cao et al. (2014). However, PIV studies focusing on human thermal plume are rare. Marr et al. (2005) studied the breathing zone flow from a thermal manikin. A planar PIV measurement of the thermal boundary layer development was studied for a standing and sitting thermal manikin, see Licina et al. (2014). A planar PIV measurement of a standing human male was also conducted, see Craven & Settles (2006). As noted above, only few of the studies involved real human subjects. Further, there has been no direct comparison of manikin and human thermal plume. Here, the measurements are carried out on a thermal manikin without breathing function and compared to the thermal plume of a real human for the first time.

2. Experimental Setup

The measurements were carried out in $80\,\mathrm{m}^2$ room containing a smaller measurement cabin. The schematic of the stereoscopic PIV experimental setup is shown in Fig. 1. The dimension of the room within the housing (measurement cabin) is $2.8\,\mathrm{m}^{\mathrm{L}} \times 2.5\,\mathrm{m}^{\mathrm{W}} \times 2.5\,\mathrm{m}^{\mathrm{H}}$. The housing has openings for camera view and the laser light-sheet. The measurement equipment including the two cameras, the laser, and the computer were placed outside the housing. The test room was unventilated. The setup was calibrated by an in-house built calibration target. The thermal manikin (average power $\approx 80\,\mathrm{W}$) was switched on 1 hour prior to the start of the experiments and the room was nebulized by DEHS particles with a mean diameter of $d_p \approx 0.4\,\mu\mathrm{m}$. It needs to be noted that the thermal manikin does not have a breathing function and incorporates only thermal convection boundary layer. The measurement plane was located $0.3\,\mathrm{m}$ above the head of the manikin. The images were recorded with Imager sCMOS cameras from LaVision GmbH (Germany) using Zeiss Makro Planar 50 mm lenses. 2000 image pairs were recorded at an image pair acquisition rate of $1\,\mathrm{Hz}$. The resulting visualization window is depicted in Fig. 1c. Further tests were also conducted with a real person and comparisons are made. The measuring system was controlled by the DaVis 10 software from LaVision GmbH, which was also utilized for data evaluation.

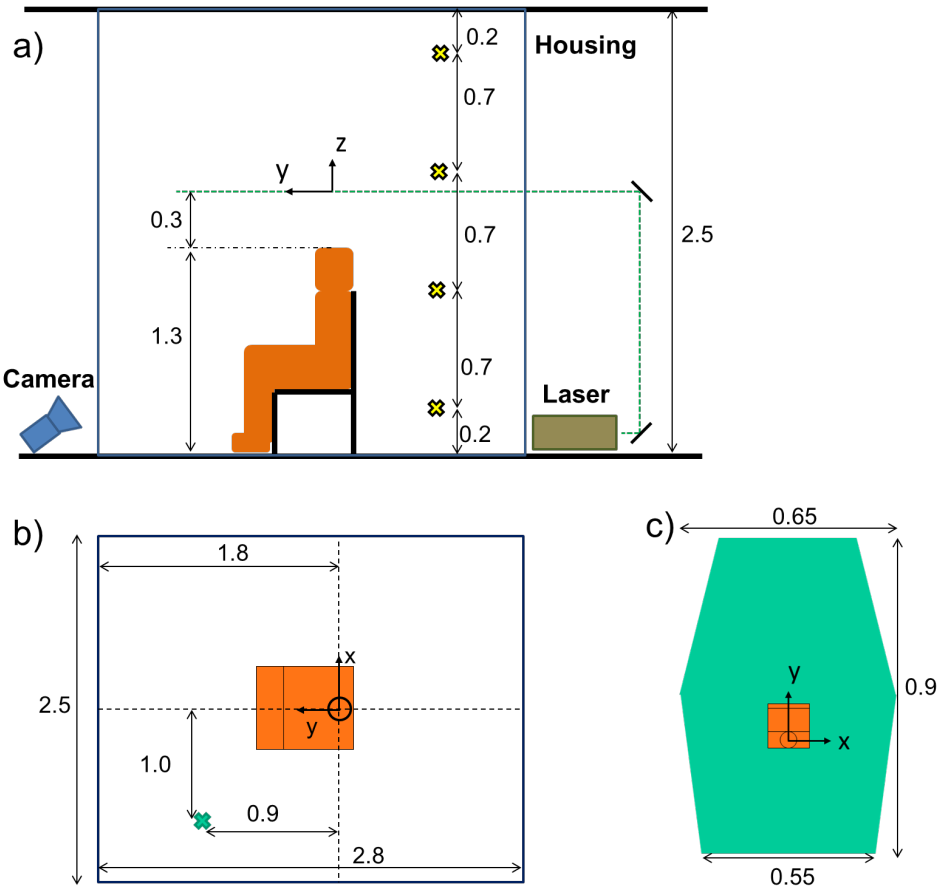

Figure 1. (a) Experimental setup for stereoscopic PIV, $\times$ sign indicates the temperature sensor position to measure room temperature gradient. (b) The top view within the housing enclosing the manikin, $\times$ sign indicates the temperature sensor position to measure room temperature at the laser height for thermal field determination (c) the visualization plane. All dimensions are in m.

One of the challenges of measuring a considerable large area of visualization is to have enough scattered light from the particles for visualization. This is solved by having the setup in forward scattering of light from particles. The laser is placed behind the thermal manikin, while the cameras are placed in the front. The forward scattering ensures high light intensities reaching the cameras. The real person was male with a height of $1.8\,\mathrm{m}$ and a weight of $75\,\mathrm{kg}$. The person was wearing formal dress with no coat on. Different scenarios of the real person were recorded: (a) normal breathing via nose, (b) talking, (c) breathing with mask on, and (d) normal breathing with person performing arm movements. Temperature measurements were carried out by PT100 sensors with accuracy of $\pm 0.03\,^{\circ}\mathrm{C}$ (1/10 DIN accuracy) and PT-104 data logger obtained from Pico Technology. The vertical room temperature gradient was measured at the four locations as shown in Fig. 1a. For measurements of temperature field above the thermal manikin, three sensors scanned the area of interest with measurement time of 15 minutes at each location. The grid for measurements is $40\,\mathrm{mm} \times 40\,\mathrm{mm}$. The average of data of the last 7.5 minutes is considered for particular location. Further, the excess temperature ΔT with respect to the room temperature at the same height (shown in Fig. 1b) is calculated.

3. Results

Figure 2 shows the velocity field of the thermal manikin and the standard deviation. The results are obtained from the average of the velocity data from the 2000 image pairs/vector fields for the thermal manikin and 1000 image pairs/vector fields for the real person cases. The center of the head is located at $x = 0$, $y = 0$. Hence it can be seen that the peak of vertical velocity is off. The results from the thermal manikin show a more distinct lobe towards the front (off centered to left) with a second maxima of the vertical velocity. This shows the effect of the plume resulting from the legs. In the case of the real person case with normal breathing (Fig. 3a), the plume reveals qualitatively similar behavior with a clear lobe towards the front. However, the peak vertical component of velocity is slightly lower in case of the real person compared to the thermal manikin. The plume axis meanders (or wanders) in time resulting in non-axisymmetric flow above the head in both the cases. Such wandering has been reported before with low temperature plumes including for human thermal plume, see Bogdan et al. (2022). The time dependent meandering was reduced with the incorporation of the housing, however does not eliminate it. This meandering effect is quantified by the standard deviation of the vertical component of the flow. Figure 3 compares the flow field for the different scenarios with the real person including normal nasal breathing, talking, breathing with mask on and person performing various actions with his hand. Figure 4 shows the corresponding standard deviation of the vertical component of the flow.

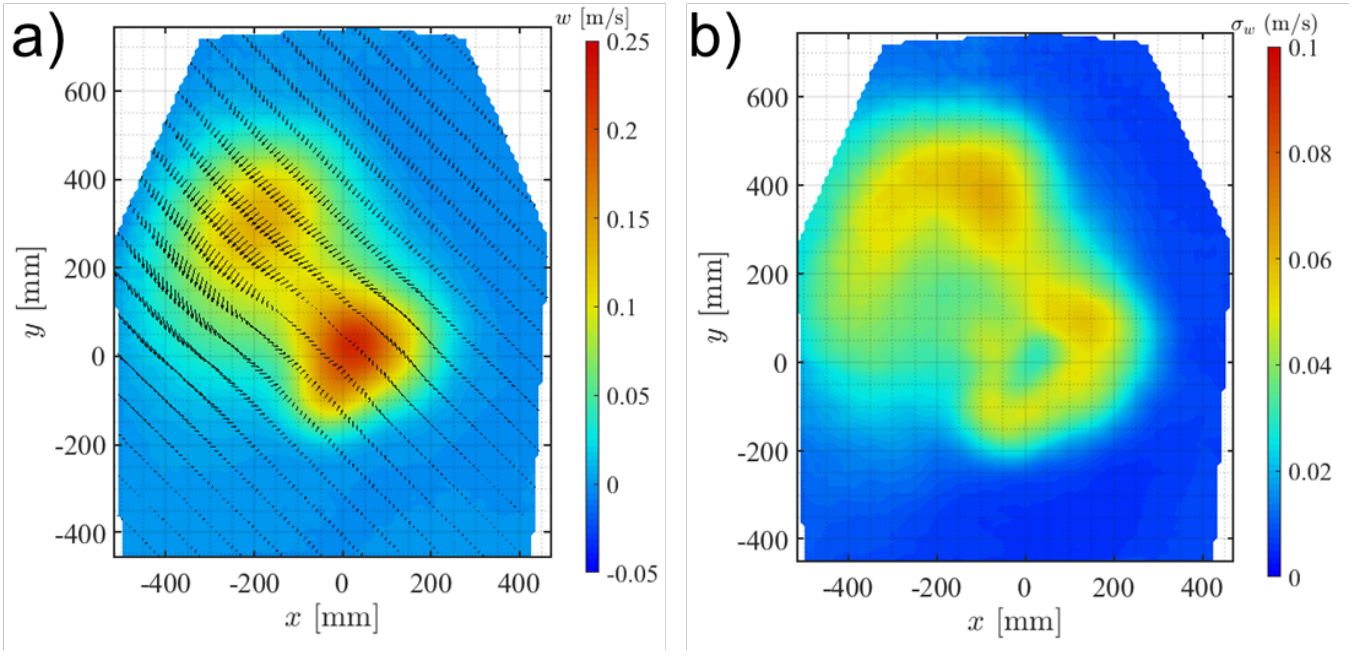

Figure 2. (a) Contour map of the w-component of the velocity above the thermal manikin with the in plane vector field overlaid. (b) Contour map of the standard deviation of the w-component of the velocity field above the thermal manikin. $x = 0$, $y = 0$ is directly above the center of the thermal manikin head. Average vertical temperature gradient in the room is $0.34\,\mathrm{K/m}$ with room temperature of $24.3\,^{\circ}\mathrm{C}$.

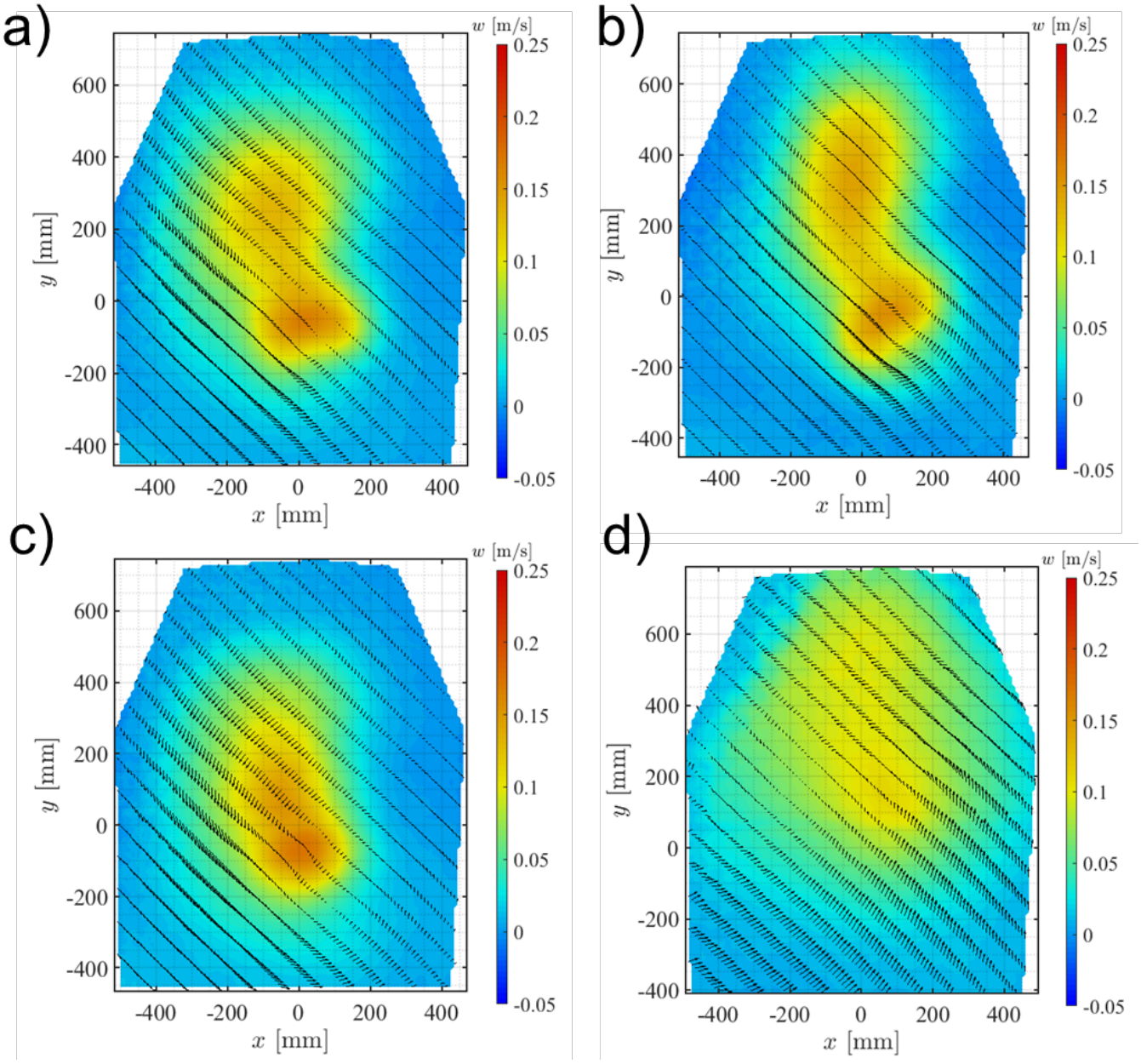

Figure 3. Contour map of the w-component of the velocity above the real person with the in-plane vector field overlaid in different scenarios: (a) normal nasal breathing, (b) talking, (c) wearing mask and (d) person doing various action with hands. $x = 0$, $y = 0$ is directly above the center of the head. Average vertical temperature gradient in the room is $0.22\,\mathrm{K/m}$ with room temperature of $25.9\,^{\circ}\mathrm{C}$.

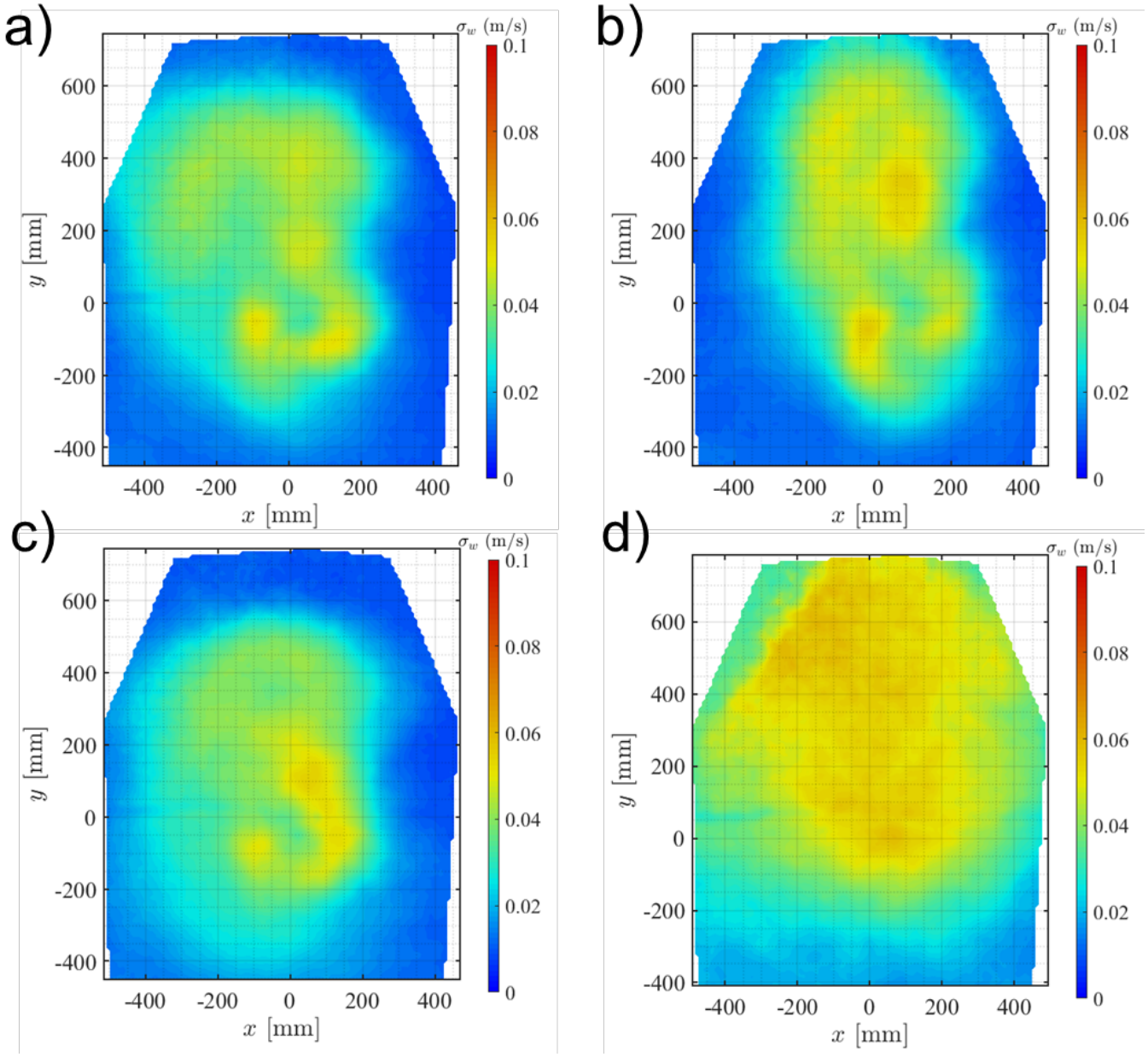

Figure 4. Contour map of the standard deviation of the w-component of the velocity field above the real person: (a) normal nasal breathing, (b) talking, (c) wearing mask and (d) person doing various action with hands. $x = 0$, $y = 0$ is directly above the center of the head.

The comparison of the human cases with different scenarios reveals that when the person is talking, the second lobe is stretched further towards the front. This indicates the effect of the further propagation of the breath while speaking. On the other hand, when the person is wearing a mask (Fig. 3c), the second lobe is further constricted and nearly merges with the plume above the head. This is consistent with the previous results, see (Kähler & Hain, 2020). With the person performing action with hand, the peak velocities has reduced, however, the spread of the vertical velocity has increased. It can also been seen that the velocity does not approach zero towards the front indicating the extent of the plume to be larger than the visualized area. Figure 4 reveals the variation

of the velocity field within the measurement time which reveals the extent of the meandering of the plume. As can be observed that the velocity field is completely captured as the standard deviation approaches zero within the visualization window. For the case of the person doing action (Fig. 4d), however, it can be seen the values are considerably higher indicating that the flow field stretches beyond the visualized window. Integral fluxes like volumetric flux V, momentum flux I, buoyancy force density P, and enthalpy flux Q are determined by Bogdan et al. (2022):

$$V = \sum w \cdot \Delta A \tag{1}$$

$$I = \rho \sum w^2 \cdot \Delta A \tag{2}$$

$$P = \rho g \beta \sum \Delta T \cdot \Delta A \tag{3}$$

$$Q = \rho C_p \sum (\Delta T w) \cdot \Delta A \tag{4}$$

where ρ is the density of air (here taken as $1.2\,\mathrm{kg/m^3}$), and w is the z-component of velocity, ΔA is the cell size, g is the acceleration due to gravity, β is the coefficient of thermal expansion of air (here taken as $0.0034\,1/\mathrm{K}$), ΔT is the excess temperature, and C_p is the heat capacity of air (here taken as 1 kJ/(kg.K)). The determined fluxes from the experimental data with real person are presented in Fig. 5. It is observed that the volumetric flux and momentum flux quantities are similar in all cases except for the person doing actions. In the case of human doing actions, the average and the standard deviation are higher. Figure 6 compares the volumetric flux and momentum flux of the real person to the case of the thermal manikin. It is observed that the volumetric flux of the manikin is slightly lower than the real person. While the momentum flux is similar in case of the thermal manikin and the real person.

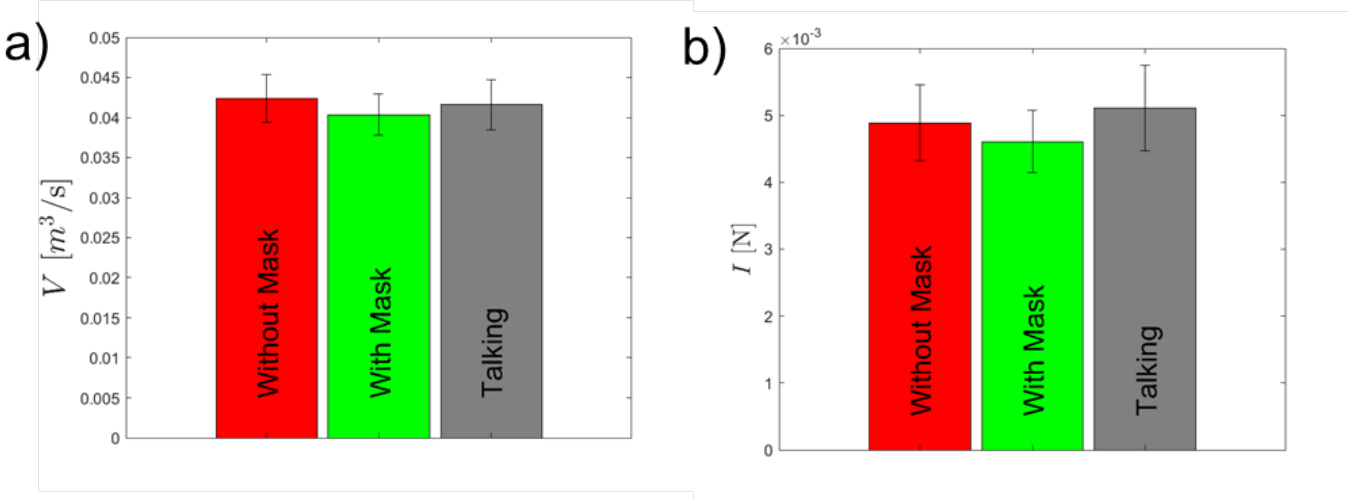

Figure 5. Comparison of the integral fluxes in case of the real person: (a) volumetric flux, and (b) momentum flux.

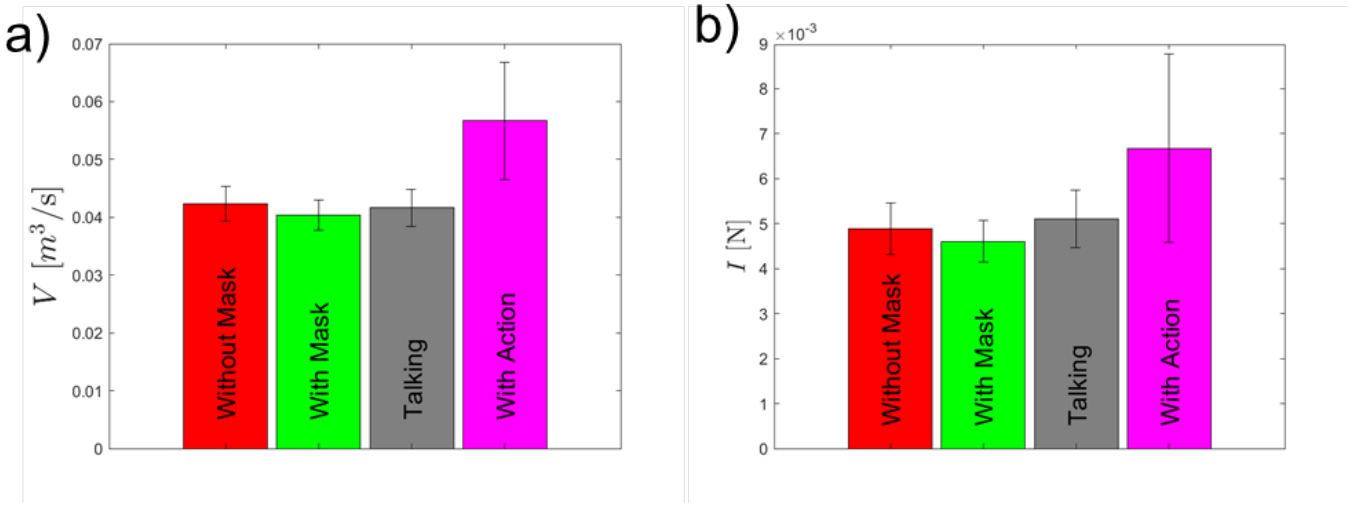

Figure 6. Comparison of the integral fluxes between the real person and the thermal manikin: (a) volumetric flux, and (b) momentum flux.

For the calculation of the buoyancy force density and the enthalpy flux, the temperature field is required. This was conducted in independent trial with the thermal manikin. The measured temperature excess above the thermal manikin is presented in Fig. 7. Similar to the velocity measurements, the peak temperature excess is off centered. Further, the lateral extent of the temperature excess is less compared to the w-component of the velocity. The derived integral buoyancy force density and enthalpy flux are $P = 0.004\,\mathrm{kg/s^2}$ and $Q = 15.5\,\mathrm{W}$ respectively. It needs to be noted that as the temperature distribution is measured over long times, the measurements are an average of the plume meandering and needs to be considered as an approximate. A similar case of thermal manikin (Power input = 72 W) with no breathing reported in literature (Zukowska et al. (2011)), the derived values are $P = 0.0042\,\mathrm{kg/s^2}$; $Q = 16.5\,\mathrm{W}$ at $0.7\,\mathrm{m}$ above the manikin. If the viscous effects are assumed negligible, then enthalpy flux above the source of the convective source is expected to be constant, see Mierzwinski (1981). It is interesting to note that the total power input to the manikin is 80 W. However, the measured enthalpy flux carried by the thermal plume is only a fraction of it ($\approx 20\,\%$). One can approximate the power lost due to thermal radiation as where is the emissivity of the body, is the Stefan's Boltzmann constant, S_1 is the surface area of the body losing heat, F_{12} is the view factor, T_1 is the temperature of the body losing heat and T_2 is the temperature of the body receiving heat. Assuming a view factor of 1 between the manikin and the room and emissivity of manikin $\epsilon = 0.9$ and the surface area of the thermal manikin is calculated to be $1.9\,\mathrm{m^2}$. For an average surface temperature of the manikin of $31\,^{\circ}\mathrm{C}$ and a room temperature of $25\,^{\circ}\mathrm{C}$, the heat lost is $Q_r = 63\,\mathrm{W}$. It needs to be emphasized that this is an example power loss due to radiation as the view factors, surface temperature and surface emissivity are approximations and not straightforward to measure the actual values. However, it clearly shows that thermal radiation dominates for such scenarios.

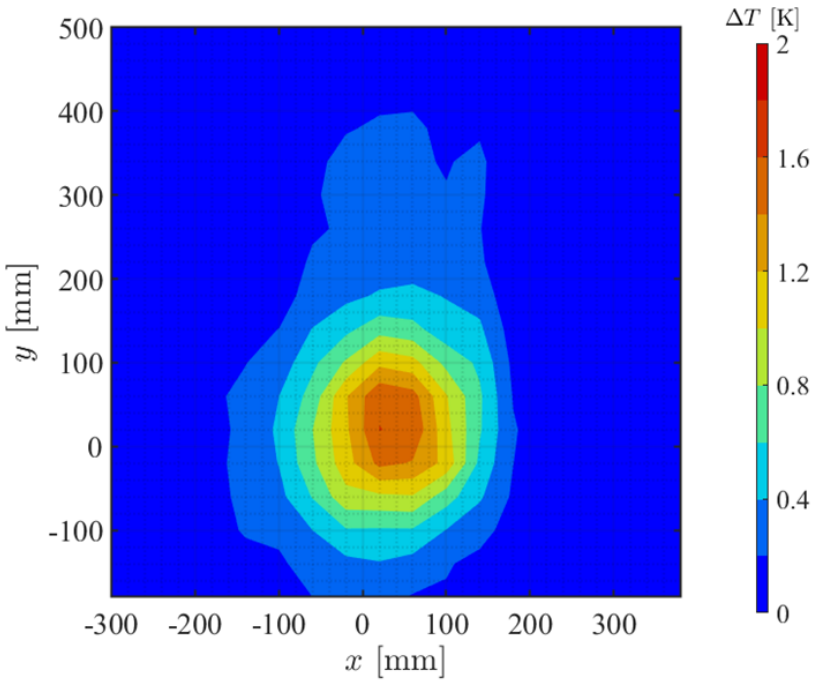

Figure 7. Temperature excess map above the thermal manikin. The room temperature is measured at the location shown in Fig. 1b.

4. Conclusions

The results presented here show that the thermal plume from a manikin without breathing function has many similarities in the average flow field above the head with the field induced by a real person. The peak velocity observed with the real person is slightly lower than the one of the thermal manikin and the structures of the thermal plumes resemble to some extent in both cases. The real person with breathing or talking revealed a bi-lobe like structure with the secondary lobe due to the breath. The thermal manikin also showed a second lobe which is due to the thermal plume from the legs. Further, the integral fluxes agree quite well. Furthermore, the effect due to breathing, speaking, and movement of the real person are discussed. The characterizations of these phenomena are important because they cannot be simulated by the manikin, while they affect the extent and strength of the thermal convection flow. Further, it is interesting to note that although the radiation from the body dominates in transfer of thermal energy from the body, the little fraction of the heat converted to convection generates significant plume. The plume might be an important safety feature in normal sitting condition as the thermal plume can transport emitted aerosol particles upwards.

Acknowledgements

The authors acknowledge funding by Die Beauftragte der Bundesregierung für Kultur and Medien (BKM) through CineCov project and dtec.bw – Digitalization and Technology Research Center of the Bundeswehr (project LUKAS). The authors also thank the Fraunhofer Institute for providing the thermal manikin for the measurements.

References

Bogdan, A., Ogłodziński, K., & Szyłak-Szydłowski, M. (2022). Analysis of thermal plumes forming over male human subjects. *Journal of Building Engineering*, *45*, 103596.

Cao, X., Liu, J., Jiang, N., & Chen, Q. (2014). Particle image velocimetry measurement of indoor airflow field: A review of the technologies and applications. *Energy and Buildings*, *69*, 367–380.

Craven, B. A., & Settles, G. S. (2006). A computational and experimental investigation of the human thermal plume. *Journal of Fluids Engineering*, *128*, 1251-1258.

Kähler, C. J., & Hain, R. (2020). Fundamental protective mechanisms of face masks against droplet infections. *Journal of aerosol science*, *148*, 105617.

Koelblen, B., & Bogdan, A. (2015). Impact of clothing, breathing and body posture on the shaping of a thermal plume above a human. *International Journal of Ventilation*, *13*(4), 397–410.

Licina, D., Pantelic, J., Melikov, A., Sekhar, C., & Tham, K. W. (2014). Experimental investigation of the human convective boundary layer in a quiescent indoor environment. *Building and Environment*, *75*, 79–91.

Marr, D., Khan, T., Glauser, M., Higuchi, H., & Zhang, J. (2005). On particle image velocimetry (piv) measurements in the breathing zone of a thermal breathing manikin. *ASHRAE Transactions*, *111*(2), 299-305.

Mierzwinski, S. (1981). Air motion and temperature distribution above a human body in result of natural convection. *A4-serien no*, *45*.

Sun, S., Li, J., & Han, J. (2021). How human thermal plume influences near-human transport of respiratory droplets and airborne particles: a review. *Environmental Chemistry Letters*, *19*(3), 1971–1982.

Zukowska, D., Melikov, A., & Popiolek, Z. (2012). Impact of personal factors and furniture arrangement on the thermal plume above a sitting occupant. *Building and Environment*, *49*, 104–116.

Zukowska, D., Melikov, A., Popiolek, Z., & Spletsteser, J. (2011). Impact of breathing on the thermal plume above a human body. In *Proceedings of the 12th international conference on air distribution in rooms–roomvent*.